Viscous flow in a slit between two elastic plates

Christensen, Anneline H.; Jensen, Kaare H.

Published in:
Physical Review Fluids

Link to article, DOI:
10.1103/physrevfluids.5.044101

Publication date:
2020

Document Version
Publisher's PDF, also known as Version of record

Viscous flow in a slit between two elastic plates

Anneline H. Christensen and Kaare H. Jensen*
Department of Physics, Technical University of Denmark, DK-2800 Kongens Lyngby, Denmark

(Received 7 February 2019; accepted 24 February 2020; published 9 April 2020)

Soft plates immersed in fluids appear in many biological processes, including swimming, flying, and breathing. The plate deforms in response to fluid flows, yet fluid stresses are in turn influenced by the plate's deformation. We present a mathematical model examining the flow of a viscous fluid in a narrow slit formed by two rectangular elastic plates, and demonstrate a strongly nonlinear flow response. The volumetric flow rate first increases linearly with pressure; however, the bending of the plates causes the corners to approach. This in turn reduces the flow rate. In some cases, the corners meet and the slit no longer permits flow. Our model, which is based on low-Reynolds-number hydrodynamics and linear plate theory, yields insights into two competing effects: While the plate bending generally reduces the slit aperture, it also causes the two plates to move apart, thus increasing the gap. Relations to biomedical flows are outlined and potential applications to flow control in man-made systems are considered.

DOI: 10.1103/PhysRevFluids.5.044101

I. INTRODUCTION

An elastic plate will bend if placed perpendicular to the flow of a fluid, a phenomenon which plays an essential role in the operation of fins, wings, heart valves, and vocal cords [1–4]. The degree of deformation will depend on the material and geometric properties of the plate and on the fluid flow. If two plates are placed opposite one another, such as in the vocal folds, the fluid will be forced to pass through the narrow slit formed by the plates, the shape of which will be influenced by the fluid stress (Fig. 1). We present theory for low-Reynolds-number flows in this system, and demonstrate a highly nonlinear relationship between the applied pressure drop Δp and the resultant flow rate Q. At low pressures, the flow rate increases linearly with pressure through the slit. At higher pressures, however, the bending and rotation of the plates causes the corners to approach. This reduces the gap size and the flow rate decreases. The topic of this paper is a detailed analysis of fluid-structure interactions in this system.

Fluid-structure interactions have a long history and many important applications within the technical, biological, and biomedical branches of science; see, e.g., [5,6] for recent reviews. Of particular relevance to the system under scrutiny here are the following studies that highlight the surprisingly diverse dynamics which arise from interactions between viscous liquids and elastic solids attached to channel boundaries. Wexler *et al.* [7] studied the bending of an elastic fiber clamped to a wall in viscous flows, while Young *et al.* [8] modeled the primary cilium as an elastic beam connected to a spring subjected to shear flow. Pozrikidis [9] simulated how single and arrays of elastic rods bend when a shear flow is passed across them. Moreover, Alvarado *et al.* [10] considered flow-induced bending of multiple soft hairs, and found a nonlinear flow impedance which they rationalized using a coupled fluid-structure model. Additionally, Gosselin *et al.* [11] carried out experiments to study the drag on flexible plates, and Duprat *et al.* [12] created a microfluidic setup

*khjensen@fysik.dtu.dk

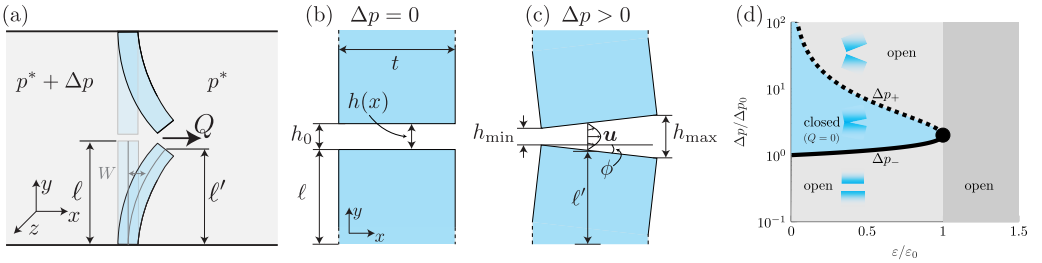

FIG. 1. Schematic of the channel geometry. (a) A pressure difference Δp drives the flow rate Q of a viscous liquid through a narrow slit between two elastic plates of height ℓ, width w, and thickness t. The elastic deformation $W(y)$ modifies the gap geometry. (b) The gap has constant height $h(x) = h_0$ when no pressure is applied. (c) When $\Delta p > 0$, elastic deformations constrict the slit; see Eqs. (9d) and (9e). (d) Phase diagram. The closing pressure Δp_- [Eq. (11b), solid line] and reopening pressure Δp_+ [Eq. (11c), dashed line] normalized by Δp_0 [Eq. (9c)] are plotted as functions of the pore-plate aspect ratio $\varepsilon = \ell h_0/t^2$ [Eq. (10d)], normalized by the critical value $\varepsilon_0 = 7/18$.

to measure mechanical properties of gels by considering the deflection of gel beams at different flow velocities. Numerous engineering applications that involve fluid flows across soft structures have been considered, including pneumatic valves [13]. Another example is Ledesma-Alonso *et al.* [14], who conducted experiments on valves consisting of two flexible plates, to study under which conditions they block backflow. Finally, Park *et al.* [15] found a nonlinear pressure-drop–flow-rate relation across a valve comprising a sphere connected to a spring in a tapering channel.

Many biological processes also take advantage of interactions between viscous liquids and elastic solids to control fluid flow by channel confinement. For instance, both heart and venous valves prevent backflows by channel occlusion, and valve dysfunction is associated with medical disorders [3,16]. During respiration—the body's cyclic intake and exhalation of air—gas flows past the slit between the vocal folds. Vocal chord dysfunction is due to transient constriction of the vocal cords during parts of the respiratory cycle [17]. While several triggers of vocal cord dysfunction have been identified, the physical mechanism of flow impediment remains poorly understood [18].

Inspired by these processes, the focus of our paper is the system shown in Fig. 1: viscous flow in a slit between two elastic plates. In particular we seek to predict the volumetric flow rate Q as function of the applied pressure Δp. We begin this paper by describing, in Sec. II, our system and propose a mathematical model for fluid-structure interactions based on geometric and material characteristics. This step allows a reduction of the model complexity to lubrication theory for the liquid flow (Sec. II A) and linear plate theory (Sec. II B) for the elastic deformations. We derive a pressure-drop versus flow rate relation (Sec. II C–II D) and conclude with a summary and discussion of our results (Sec. III).

II. RESULTS

The system under consideration consists of a long channel with two rectangular plates of thickness t and height $\ell \gg t$ extending from the top and bottom walls as shown schematically in Figs. 1(a) and 1(b). The two plates are separated by a slit of height h_0 which is significantly smaller than the plate thickness t. The fluid flows in the x direction and the plates extend in the y direction. The plates are flexible and the flow of a Newtonian fluid of viscosity η and density ρ is driven by an applied pressure difference Δp across the gap. The width of the channel and plates along the z direction is $w \gg \ell$, making the problem essentially two-dimensional. The dynamics of the fluid are described by the Navier-Stokes and continuity equations:

$$\rho(\partial_t \boldsymbol{u} + \boldsymbol{u} \cdot \boldsymbol{\nabla}\boldsymbol{u}) = -\nabla p + \eta \nabla^2 \boldsymbol{u}, \tag{1}$$

$$\boldsymbol{\nabla} \cdot \boldsymbol{u} = 0, \tag{2}$$

where $\boldsymbol{u} = (u_x, u_y)$ is the two-dimensional velocity field and p is the pressure. Throughout our analysis, we assume that the channel aspect ratio $h_0/t \ll 1$ and that the ratio of inertial forces $\rho u^2/t$ to viscous forces $\eta u/h_0^2$ is small, i.e., $\rho u h_0^2/(t\eta) \ll 1$. In this limit, we can safely neglect the inertial terms and use the Stokes' equations and the lubrication approximation thereof to describe the hydrodynamics. We note that the asymptotic relative error in these approximations is the aspect ratio squared, $O(h_0^2/t^2)$. Next we consider the deformation of the plates where balance of stresses in the solid leads to $\nabla \cdot \boldsymbol{\sigma} = 0$ and the boundary condition at the solid-fluid interface is $\boldsymbol{\sigma} \cdot \boldsymbol{n} = -p\boldsymbol{n}$. In this analysis, we assume that the horizontal deflection is small relative to the plate thickness, so that a linear elastic theory suffices to describe the material response.

A. Low-Reynolds-number flow

The pressure p and the velocity field $\boldsymbol{u}$ in the slit are described by the lubrication equations

$$\frac{\partial p}{\partial x} = \eta \frac{\partial^2 u_x}{\partial y^2}, \tag{3a}$$

$$\frac{\partial p}{\partial y} = 0, \tag{3b}$$

$$\frac{\partial u_x}{\partial x} + \frac{\partial u_y}{\partial y} = 0. \tag{3c}$$

In the local slit coordinate system, $y = 0$ corresponds to the channel centerline, while $x = 0$ is located at the channel entrance. Assuming no-slip boundary conditions at the edges of the pore ($y = \pm h(x)/2$), the horizontal velocity component is found as

$$u_x(x, y) = \frac{1}{2\eta} \frac{\partial p}{\partial x} \left(y^2 - \frac{y h(x)}{2} \right), \tag{4}$$

corresponding to the flow rate

$$Q = -\frac{w}{12\eta} \frac{\partial p}{\partial x} h^3(x). \tag{5}$$

The pressure-drop versus flow-rate relation is found by integration across the slit along the x direction:

$$\Delta p = \frac{12\eta Q}{w} \int_a^b h^{-3}(x)\, dx, \tag{6}$$

where $x = a$ and $x = b$ are the inlet and outlet positions on the x axis, respectively. The hydraulic resistance $R = \Delta p/Q$ of the undeformed pore is

$$R_0 = \frac{12\eta t}{w h_0^3}. \tag{7}$$

B. Elastic deformation of the plate

To characterize the change in the slit geometry with applied pressure, we consider the horizontal deflection W of the lower plate. In the local coordinate system, $y = 0$ is located at the base of the clamped plate while the tip at $y = \ell$ is free to move. Stress balance in the solid yields the one-dimensional Föppl–von Kármán plate equation [19]

$$D \frac{\partial^4 W}{\partial y^4} - t \frac{\partial}{\partial y} \left(T \frac{\partial W}{\partial y} \right) = \Delta p, \tag{8a}$$

where D is the flexural rigidity,

$$D = \frac{Et^3}{12(1-\nu^2)}, \tag{8b}$$

T is the tension along the plate, and E and ν are Young's modulus and Poisson's ratio of the plate, respectively. Note that the ends are free, and the tension throughout the plate is $T = 0$. The pressure is treated as uniform on the plate face [20], and we neglect the effects of horizontal shear forces in the narrow slit. These scale as $\int \eta \partial_y u_x \, dx \sim \eta u_x t/h_0 \sim \Delta p h_0$, which is much smaller than the pressure force $\Delta p \ell$ on the vertical plate surface. The boundary conditions are

$$W(0) = W'(0) = W''(\ell) = W'''(\ell) = 0, \tag{8c}$$

corresponding to clamped edges at the channel walls ($y = 0$) and free edges at the slit ($y = \ell$). Solving Eq. (8a) with $T = 0$ and the boundary conditions of Eq. (8c) leads to

$$W(y) = \frac{(6\ell^2 y^2 - 4\ell y^3 + y^4)}{24D}\Delta p. \tag{8d}$$

If the deformations are small, the horizontal plate face remains flat in accord with Kirchoff's hypothesis of straight normals. The height profile $h(x)$ of the slit between the two opposing plates is thus a linear function of position x, which we write as

$$h(x) = h_{\min} + 2x\tan\phi \quad \text{for } 0 < x < t\cos\phi, \tag{9a}$$

where $h_{\min}$ is the minimum gap size and ϕ is the tilt angle [Fig. 1(c)]. For clarity in the geometric interpretation we express the following results in terms of trigonometric functions. Note, however, that, because the deformations are small, the tilt angle ϕ is also small and the functions are approximated as $\tan\phi = \sin\phi = \phi$, $\cos\phi = 1$, etc., consistent with linear elasticity theory. The angle ϕ is determined by evaluating the deflection at the free end of the plate,

$$\tan\phi = \partial_y W|_{y=\ell} = \frac{h_0}{t}\frac{\Delta p}{\Delta p_0}, \tag{9b}$$

where we have introduced the characteristic pressure Δp_0 at which the pore closes if the motion is purely rotational:

$$\Delta p_0 = \frac{E}{2(1-\nu^2)}\frac{t^2 h_0}{\ell^3}. \tag{9c}$$

The minimum (and maximum) plate-to-plate separation distance follows from geometric considerations [Fig. 1(c)]:

$$h_{\min} = 2\ell + h_0 - 2\left(\ell' + \frac{t}{2}\sin\phi\right) = h_0 + 2(\ell - \ell') - t\sin\phi \quad \text{and} \tag{9d}$$

$$h_{\max} = 2\ell + h_0 - 2\left(\ell' - \frac{t}{2}\sin\phi\right) = h_0 + 2(\ell - \ell') + t\sin\phi. \tag{9e}$$

The two main competing effects in the fluid-structure interaction process are contained in Eq. (9d). First, the two leading-edge corners of the top and bottom plates begin to approach as the plates bend. Quantitatively, the angle ϕ increases and the absolute magnitude of the term $-t\sin\phi$ grows. Thus $h_{\min}$ diminishes linearly with pressure. However, since the length of each plate is unaltered by the bending process, they retract to a new effective length ℓ'. Thus, $h_{\min}$ increases by a term $2(\ell - \ell')$. The projected length ℓ' of the deflected plate on the y axis can be found by considering the arch

length of the plate center line, which should equal the equilibrium plate height ℓ:

$$\ell = \int_0^{\ell'} \sqrt{1 + (\partial_y W)^2}\, dy, \tag{10a}$$

which, in the small slope limit $\partial_y W \ll 1$, leads to

$$\ell' \simeq \ell \left[1 - \frac{9}{28} \frac{h_0^2}{t^2} \left(\frac{\Delta p}{\Delta p_0} \right)^2 \right]. \tag{10b}$$

The relative retraction K can be expressed as

$$K = 2\frac{\ell - \ell'}{h_0} = \frac{1}{4}\frac{\varepsilon}{\varepsilon_0} \left(\frac{\Delta p}{\Delta p_0} \right)^2, \tag{10c}$$

where we have introduced the parameters

$$\varepsilon = \frac{\ell h_0}{t^2} \quad \text{and} \quad \varepsilon_0 = \frac{7}{18} \approx 0.389, \tag{10d}$$

where ε is the ratio of the channel and plate aspect ratios, h_0/t and t/ℓ, respectively.

The gap will close ($h_{\min} = 0$) if a real pressure drop Δp can be found such that

$$h_0 + 2[\ell - \ell'(\Delta p)] - t \sin \phi(\Delta p) = 0, \tag{11a}$$

where we emphasize that the projected plate length ℓ' [Eq. (10b)] and tip angle ϕ [Eq. (9b)] are pressure dependent. The potential closure, and reopening, of the pore can thus be characterized by the critical pressures at which $h_{\min} = 0$, i.e.,

$$\Delta p_- = \frac{2\varepsilon_0}{\varepsilon} \left(1 - \sqrt{1 - \frac{\varepsilon}{\varepsilon_0}} \right) \Delta p_0, \tag{11b}$$

$$\Delta p_+ = \frac{2\varepsilon_0}{\varepsilon} \left(1 + \sqrt{1 - \frac{\varepsilon}{\varepsilon_0}} \right) \Delta p_0, \tag{11c}$$

where the indices indicate closing ($-$) and reopening ($+$) of the pore. We note the importance of the geometric parameter ε in Eqs. (11c) and (11b): the pressures $\Delta p_\pm$ are real when $\varepsilon < \varepsilon_0$, hence there is a range of Δp for which the slit is open, closed, and reopens. In contrast, for $\varepsilon > \varepsilon_0$ the retraction is sufficiently strong that the channel remains open for all pressures; see the phase diagram in Fig. 1(d).

We end our discussion of the closing process by discussing limits to the value of the geometric parameters in the problem. The rotation must be small for the one-dimensional plate equation to hold, i.e., $W'(\ell) \ll 1$ or equivalently $\phi \ll 1$. Further, the lubrication approximation dictates that the channel height must remain well below the channel thickness t. Taking the global assumption that $h_0/t \ll 1$ leads to the conditions

$$\phi = \frac{h_0}{t}\frac{\Delta p}{\Delta p_0} \ll 1 \quad \text{and} \quad \frac{h_{\max}}{t} = \frac{\ell h_0^2}{t^3} \left(\frac{\Delta p}{\Delta p_0} \right)^2 \ll 1. \tag{12}$$

We note that the whole (ε, Δp) parameter space can be reached provided that the aspect ratios h_0/t and t/ℓ are chosen judiciously.

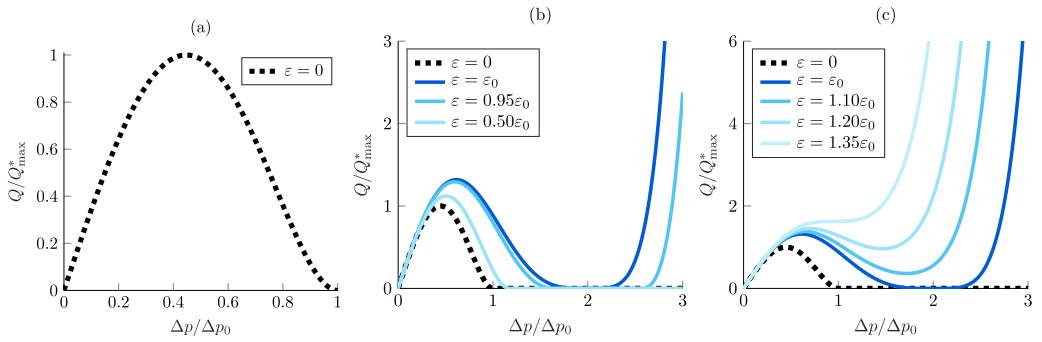

FIG. 2. Pressure-drop versus flow-rate characteristics. Flow rate Q [Eq. (13b)] plotted as a function of pressure drop Δp. The flow is normalized by the maximum rate $Q^*_{\max}$ [cf. Eq. (14b)], while the pressure is normalized by the characteristic pressure Δp_0 [Eq. (9c)]. (a) Pressure-drop versus flow-rate relation in the limit $\varepsilon = 0$ [Eq. (14a)]. (b) Flow characteristics below the critical value $\varepsilon < \varepsilon_0 = 7/18$ where the slit closes at Δp_- and subsequently reopens at Δp_+ [cf. Eqs. (11b) and (11c)]. (c) System behavior for $\varepsilon > \varepsilon_0$ where the slit remains open for all Δp. Note that, at the critical value $\varepsilon = \varepsilon_0$, the slit closes and reopens at the same pressure $\Delta p = \Delta p_\pm = 2\Delta p_0$. See also the phase diagram in Fig. 1(d).

C. Flow-rate versus pressure-drop characteristics

Having established the height profile of the deformed slit, we return to the pressure-drop versus flow-rate relation in Eq. (6). The pressure drop obtained with the height profile of the distorted channel [Eq. (9a)] is

$$\Delta p = \frac{12\eta Q}{w}\int_0^{t\cos\phi} h^{-3}(x)\,dx = \frac{12\eta Q}{w}\frac{1}{4\tan\phi}\left(h_{\min}^{-2} - h_{\max}^{-2}\right). \tag{13a}$$

Inserting the expressions for the maximum and minimum gap height, Eqs. (9d) and (9e), the flow rate Q as a function of pressure difference Δp becomes

$$Q = \frac{\Delta p}{R_0}(1+K)^3\left[1 - \left(\frac{1}{1+K}\frac{\Delta p}{\Delta p_0}\right)^2\right]^2, \tag{13b}$$

where $K(\Delta p)$ is the relative retraction [Eq. (10c)] and R_0 is the hydraulic resistance of the unperturbed slit [Eq. (7)]. Note that $Q = 0$ for pressures in the closed state $\Delta p_- < \Delta p < \Delta p_+$ [Eqs. (11b) and (11c)].

The characteristic behavior of the flow rate Q as function of applied pressure Δp is illustrated in Fig. 2 for different values of the geometric parameter $\varepsilon = \ell h_0/t^2$. We first note that when $\varepsilon \to 0$ the relative retraction K is significantly smaller than unity and the pressure-drop versus flow-rate relation in Eq. (13b) simplifies to

$$Q^* = \frac{\Delta p}{R_0}\left[1 - \left(\frac{\Delta p}{\Delta p_0}\right)^2\right]^2. \tag{14a}$$

In this limit, the flow rate initially increases linearly with Δp [Fig. 2(a)]. At higher pressures, however, the bending of the plates reduces the gap size and the flow rate decreases. Finally, the flow rate tends to zero as the two plates approach contact at $\Delta p = \Delta p_0$. The maximum flow rate in this limit is

$$Q^*_{\max} = \frac{16}{25\sqrt{5}}\frac{\Delta p_0}{R_0}, \tag{14b}$$

obtained when the pressure $\Delta p = \Delta p_0/\sqrt{5}$. For larger values of ε, the plate retraction is significant and we observe a transition between closing, reopening, and perpetually open slits beyond the critical value $\varepsilon > \varepsilon_0 = 7/18$ [Figs. 2(b) and 2(c); see also the phase diagram in Fig. 1(d)].

The preceding analysis focused on the flow rate Q as function of the applied pressure difference Δp and revealed a strongly nonlinear relationship between the two [Eq. (13b)]. Crucially, we found that the link between flow $Q(\Delta p)$ and pressure Δp is unique. However, the situation is qualitatively different if we consider the flow rate Q as the prescribed quantity and seek the corresponding pressure drop $\Delta p(Q)$. Here, the functional relationship is no longer one-to-one because some flow rates correspond to one, two, or three pressure values. In the following, we thus briefly consider the stability of the prescribed flow-rate case.

Let Q_1 be the constant volumetric flow rate entering the system, which at steady-state corresponds to the pressure drop Δp_1. If a small perturbation to the plate position occurs, volume conservation dictates that

$$Q_1 = Q(\Delta p) + \frac{\partial V}{\partial t}, \tag{15a}$$

where Q is the flow through the slit, Δp is the pressure drop across the plates, V is the channel volume behind the plates, and t is time. Starting at the initial value V_0 at $\Delta p = 0$, the volume V grows linearly with pressure as the plates bend, i.e., $V = V_0 + \alpha \Delta p$, where the positive constant α follows from Eq. (8d). Rewriting the volume term in Eq. (15a) and expanding near the steady state pressure Δp_1 leads to

$$\alpha \frac{\partial}{\partial t}(\Delta p - \Delta p_1) = Q_1 - Q \approx Q_1 - \left[Q_1 + (\Delta p - \Delta p_1) \left.\frac{\partial Q}{\partial \Delta p}\right|_{\Delta p_1} \right] = -(\Delta p - \Delta p_1) \left.\frac{\partial Q}{\partial \Delta p}\right|_{\Delta p_1}. \tag{15b}$$

We observe that positive values of the local resistance $\partial Q/\partial \Delta p$ are stable, while negative values are unstable. In the constant-flow case, the downward-sloping segment of the $(\Delta p, Q)$ curve is thus unstable (Fig. 2).

D. The effects of plate shape

Up to this point we have considered elastic plates with straight horizontal edges. It is, however, of general interest to consider the behavior of plates with curved boundaries. For instance, they may be easier to fabricate and align in an experiment.

We let $F(\bar{x})$ be the shape function such that the distance between the two unbent plates is $H(x) = h_0(1 + 2F(\bar{x}))$ with $\bar{x} = x/t$; see Fig. 3(a). For the case of rectangular plates with straight edges $F(\bar{x}) = 0$, and the distance between the plates is $H(x) = h_0$. The maximum value the function $h_0 F(\bar{x})$ can take is small compared to the vertical extent, ℓ, of the plates, such that the moment of inertia is unaffected and the deflection as found by Eq. (8d) still holds. Moreover, we assume that only small deflections occur so the hypothesis of straight normals remains valid. Therefore, the horizontal edge of the plate will retain its shape during the deformation. The distance between the two plates in the bent state is therefore $H(x) = h(x) + 2h_0 F(\bar{x})$, where $h(x)$ is given in Eq. (9a). This leads to

$$H(x) = h_0 + 2(\ell - \ell') - t \sin\phi + 2x \tan\phi + 2h_0 F(\bar{x}), \tag{16a}$$

which can be conveniently expressed in terms of the parameters ε and Δp_0 as

$$H(x) = h_0 \left(1 + \frac{1}{4} \frac{\varepsilon}{\varepsilon_0} \frac{\Delta p^2}{\Delta p_0^2} + [2\bar{x} - 1] \frac{\Delta p}{\Delta p_0} + 2F(\bar{x}) \right). \tag{16b}$$

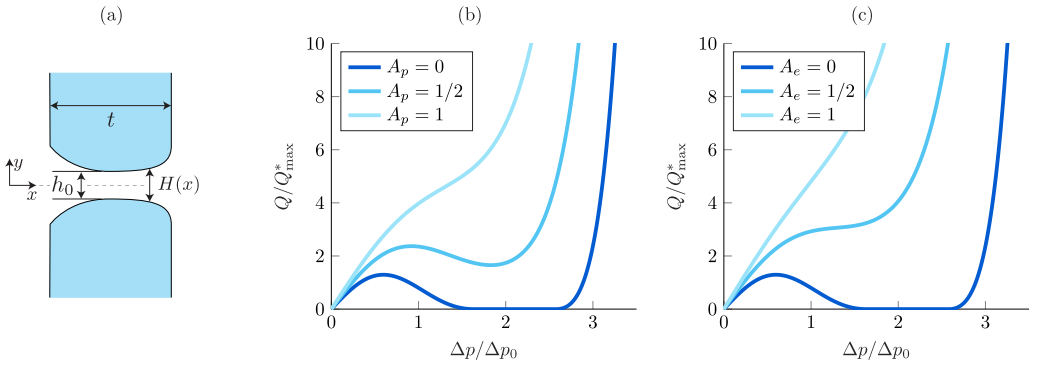

FIG. 3. Pressure-drop versus flow-rate characteristics for shape-perturbed slits (a). Flow rate Q [Eq. (17)] plotted as a function of pressure drop Δp for $\varepsilon = 0.95\varepsilon_0$. The flow is normalized by the maximum rate $Q^*_{\max}$ [cf. Eq. (14b)], while the pressure is normalized by the characteristic pressure Δp_0 [Eq. (9c)]. (b) Pressure-drop versus flow-rate relation for a parabolic shape perturbation [Eq. (18)]. (c) Pressure-drop versus flow-rate relation for an elliptical shape perturbation [Eq. (18)].

The flow rate as a function of pressure difference can then be found by inserting $H(x)$ into the expression found from the lubrication approximation in Eq. (6):

$$Q = \frac{\Delta p}{R_0}\left[\int_0^1 \left(\frac{H}{h_0}\right)^{-3} d\bar{x}\right]^{-1}. \tag{17}$$

If the ends are straight [$F(\bar{x}) = 0$] we recover Eq. (13b); however, in the general case of an arbitrary channel height profile the integral is evaluated numerically.

To illustrate the behavior of the system we consider parabolic and elliptic shape functions

$$F_p(\bar{x}) = A_p\left(\bar{x} - \frac{1}{2}\right)^2 \quad \text{and} \quad F_e(\bar{x}) = A_e\left(\frac{1}{2} - \sqrt{\bar{x}(1-\bar{x})}\right), \tag{18}$$

where A denotes the amplitude of the perturbation. Typical flow rates characteristics obtained by using Eq. (18) in Eq. (17) are shown in Fig. 3. For the geometric control parameter $\varepsilon = 0.95\varepsilon_0$, the plates with straight ends will meet, and hence the flow rate will reach zero across a finite pressure range. For relatively small values of A the same behavior is observed in shape-perturbed channels. However, for larger values of A the plates no longer come into contact and the flow rate does not reach zero for any pressure difference across the plates. Finally, we note that the flow in perturbed channels is greater ($A > 0$) or smaller ($A < 0$) than in the corresponding channel, because a wider channel permits more flow.

III. DISCUSSION AND CONCLUSION

A fairly comprehensive picture of the elements that influence viscous flow in the gap between two elastic plates has come into view. Most prominent is the discovery that this simple system can act as a nonlinear valve with remarkably complex properties [Fig. 1(d)]. The flow rate first increases linearly with pressure; however, the bending of the plates eventually reduces the gap size and the flow rate is reduced. Then, the gap closes and no longer permits flow. Finally, the pore reopens at a higher pressure. The behavior is symmetric in the applied pressure Δp, i.e., the same behavior, but with reversed flow, would be observed under the application of a negative pressure drop. It is worth mentioning that a simplification where a rigid boundary along the symmetry axis replaces the lower half of the setup would lead to the same overall behavior, but with different numerical prefactors.

The qualitative behavior of the system is captured by the geometric control parameter ε [Eq. (10d)] and the closing pressure Δp_0 [Eq. (9c)]. The quantitative properties depend on the material and geometric parameters of the system. The closing pressure is determined by the height ℓ and thickness t of the plates, the initial gap h_0, and on and the elastic parameters E and ν. The maximum achievable flow rate [Eq. (14b)] also depends on the slit width w; hence the two parameters can be controlled independently. We note that the full problem presented in Fig. 1 could be solved for individual cases using, for instance, a finite-element package. This solution method could, in principle, capture higher degrees of membrane and pore deformation and the corresponding three-dimensional flow fields [21].

Flows across soft plates are an integral part of numerous natural and technical processes. Our results could find applications in describing, for instance, the flow dynamics in the vocal folds below the phonation threshold pressure, the minimum lung pressure required to initiate and sustain vocal fold oscillations [22]. Moreover, it could help rationalize aspects of vocal chord dysfunction, in particular the transient constriction of the vocal cords during respiration [17,18]. Finally, we propose that the nonlinear flow properties of the system under consideration could find applications in, for example, flow control in lab-on-a-chip systems where efficient valve design remains a significant challenge [23,24].

ACKNOWLEDGMENTS

The authors wish to thank Ya Gai and Howard A. Stone for stimulating discussions and two anonymous referees for their constructive suggestions. This work was supported by a research grant (13166) from Villum Fonden.

[1] Z. Zhang, Mechanics of human voice production and control, J. Acoust. Soc. Am. **140**, 2614 (2016).
[2] M. Gazzola, M. Argentina, and L. Mahadevan, Scaling macroscopic aquatic locomotion, Nat. Phys. **10**, 758 (2014).
[3] F. Sotiropoulos, T. B. Le, and A. Gilmanov, Fluid mechanics of heart valves and their replacements, Annu. Rev. Fluid Mech. **48**, 259 (2016).
[4] T. Y. Wu, Fish swimming and bird/insect flight, Annu. Rev. Fluid Mech. **43**, 25 (2011).
[5] C. Duprat and H. A. Stone, *Fluid-Structure Interactions in Low-Reynolds-Number Flows* (Royal Society of Chemistry, London, 2015).
[6] E. H. Dowell and K. C. Hall, Modeling of fluid-structure interaction, Annu. Rev. Fluid Mech. **33**, 445 (2001).
[7] J. S. Wexler, P. H. Trinh, H. Berthet, N. Quennouz, O. du Roure, H. E. Huppert, A. Lindner, and H. A. Stone, Bending of elastic fibres in viscous flows: The influence of confinement, J. Fluid Mech. **720**, 517 (2013).
[8] Y.-N. Young, M. Downs, and C. R. Jacobs, Dynamics of the primary cilium in shear flow, Biophys. J. **103**, 629 (2012).
[9] C. Pozrikidis, Shear flow past slender elastic rods attached to a plane, Int. J. Solids Struct. **48**, 137 (2011).
[10] J. Alvarado, J. Comtet, E. de Langre, and A. Hosoi, Nonlinear flow response of soft hair beds, Nat. Phys. **13**, 1014 (2017).
[11] F. Gosselin, E. De Langre, and B. A. Machado-Almeida, Drag reduction of flexible plates by reconfiguration, J. Fluid Mech. **650**, 319 (2010).
[12] C. Duprat, H. Berthet, J. S. Wexler, O. Du Roure, and A. Lindner, Microfluidic in situ mechanical testing of photopolymerized gels, Lab Chip **15**, 244 (2015).
[13] M. A. Unger, H.-P. Chou, T. Thorsen, A. Scherer, and S. R. Quake, Monolithic microfabricated valves and pumps by multilayer soft lithography, Science **288**, 113 (2000).
[14] R. Ledesma-Alonso, J. Guzmán, and R. Zenit, Experimental study of a model valve with flexible leaflets in a pulsatile flow, J. Fluid Mech. **739**, 338 (2014).

[15] K. Park, A. Tixier, A. Christensen, S. Arnbjerg-Nielsen, M. Zwieniecki, and K. Jensen, Viscous flow in a soft valve, J. Fluid Mech. **836**, R3 (2018).
[16] Y. Qui, R. Quijano, S. Wang, and N. H. Hwang, Fluid dynamics of venous valve closure, Ann. Biomed. Eng. **23**, 750 (1995).
[17] N. M. Dunn, R. K. Katial, and F. C. Hoyte, Vocal cord dysfunction: A review, Asthma Res. Pract. **1**, 9 (2015).
[18] M. Weinberger and D. Doshi, Vocal cord dysfunction: A functional cause of respiratory distress, Breathe **13**, 15 (2017).
[19] S. Timoshenko and J. Goodier, *Theory of Elasticity* (McGraw-Hill, New York, 1969).
[20] H. Hasimoto, On the flow of a viscous fluid past a thin screen at small Reynolds numbers, J. Phys. Soc. Jpn. **13**, 633 (1958).
[21] G. Hou, J. Wang, and A. Layton, Numerical methods for fluid-structure interaction—A review, Commun. Comput. Phys. **12**, 337 (2012).
[22] R. W. Chan and I. R. Titze, Dependence of phonation threshold pressure on vocal tract acoustics and vocal fold tissue mechanics, J. Acoust. Soc. Am. **119**, 2351 (2006).
[23] K. Oh and C. Ahn, A review of microvalves, J. Micromech. Microeng. **16**, R13 (2006).
[24] M. J. Felton, The new generation of microvalves, Anal. Chem. **75**, 429 (2003).